Cellular and Molecular Life Sciences (2025) 82:48
https://doi.org/10.1007/s00018-024-05573-w

ORIGINAL ARTICLE

N^6-Methylandenosine-related lncRNAs as potential biomarkers for predicting prognosis and the immunotherapy response in pancreatic cancer

Zhihui Bai[1,2] · Qianlin Xia[3] · Wanli Xu[1] · Zhirong Wu[4] · Xiaomeng He[5] · Xin Zhang[1] · Zhefeng Wang[2,6] · Mengting Luo[1] · Huaqin Sun[1] · Songmei Liu[7] · Jin Wang[1,2,5]

Received: 27 November 2024 / Revised: 20 December 2024 / Accepted: 30 December 2024

Abstract

Emerging evidence has shown that the N^6-methyladenosine (m^6A) modification of RNA plays key roles in tumorigenesis and the progression of various cancers. However, the potential roles of the m^6A modification of long noncoding RNAs (lncRNAs) in pancreatic cancer (PaCa) are still unknown. To analyze the prognostic value of m^6A-related lncRNAs in PaCa, an m6A-related lncRNA signature was constructed as a risk model *via* Pearson's correlation and univariate Cox regression analyses in The Cancer Genome Atlas (TCGA) database. The tumor microenvironment (TME), tumor mutation burden, and drug sensitivity of PaCa were investigated by m^6A-related lncRNA risk score analyses. We established an m^6A-related risk prognostic model consisting of five lncRNAs, namely, LINC01091, AC096733.2, AC092171.5, AC015660.1, and AC005332.6, which not only revealed significant differences in immune cell infiltration associated with the TME between the high-risk and low-risk groups but also predicted the potential benefit of immunotherapy for patients with PaCa. Drugs such as WZ8040, selumetinib, and bortezomib were also identified as more effective for high-risk patients. Our results indicate that the m^6A-related lncRNA risk model could be an independent prognostic indicator, which may provide valuable insights for identifying therapeutic approaches for PaCa.

Keywords Pancreatic cancer · lncRNA · m6A · Prognosis · Immunotherapy

Zhihui Bai and Qianlin Xia contributed equally to this work.

✉ Jin Wang
wang.jin@zsxmhospital.com

1 Central Laboratory, Zhongshan Hospital (Xiamen), Fudan University, Xiamen 361015, China

2 Xiamen Key Laboratory of Biotherapy, Xiamen 361015, China

3 Laboratory Medicine, Shanghai Sixth People's Hospital Affiliated with Shanghai Jiao Tong University School of Medicine, Shanghai 200233, China

4 Department of General Surgery, Zhongshan Hospital (Xiamen), Fudan University, Xiamen 361015, China

5 Shanghai Public Health Clinical Center, Fudan University, 2901 Caolang Road, Jinshan District, Shanghai, China

6 Clinical Research Center for Precision Medicine of Abdominal Tumor of Fujian Province, Xiamen, China

7 Department of Clinical Laboratory, Center for Gene Diagnosis & Program of Clinical Laboratory, Zhongnan Hospital of Wuhan University, Wuhan, China

Abbreviations

AUC	Area under the curve
CI	Confidence interval
DCA	Decision curve analysis
ECM	Extracellular matrix
EMT	Epithelial to mesenchymal transition
GO	Gene ontology
HLA	Human leukocyte antigen
KEGG	Kyoto encyclopedia of genes and genomes
lncRNAs	Long non-coding RNAs
LUAD	Lung adenocarcinoma
m^6A	N^6-methyladenosine
MHC	Major histocompatibility complex
OS	Overall survival
PaCa	Pancreatic cancer
ROC	Receiver operating characteristic
TIICs	Tumor-infiltrating immune cells
TMB	Tumor mutation burden
TME	Tumor microenvironment

Published online: 21 January 2025

Introduction

Pancreatic cancer (PaCa) is the most common malignant gastrointestinal malignancy and is known for its aggressive behavior and high metastatic potential [1]. Most patients are diagnosed at an advanced stage and miss the opportunity for surgical intervention [2], and the 5-year survival rate for most highly aggressive PaCa patients in the United States is approximately 5% [3, 4]. Therefore, identifying effective prognostic biomarkers for therapeutic targets to reduce mortality in patients with PaCa is crucial.

Long noncoding RNAs (lncRNAs), which are RNA molecules with transcript lengths greater than 200 nucleotides that do not encode proteins [5, 6], can serve as novel blood-based biomarkers of disease and potential targets of therapeutic strategies for PaCa [7] and are epigenetic regulators of epithelial to mesenchymal transition (EMT) in PaCa [8]. They also play key roles in the initiation and progression of PaCa through complex regulatory networks that involve transcriptional regulation, epigenetic modifications, and posttranslational modifications. Therefore, lncRNAs have gradually attracted our attention [6, 9].

As the most characteristic and common posttranscriptional chemical modification, N^6-methyladenosine (m^6A) occurs at the N^6 position of adenosine and represents the most abundant posttranscriptional modification in both mRNAs and noncoding RNAs in mammals [10]. The dynamic regulation of m^6A modifications in cancer is mediated by three main types of proteins, namely, writers, erasers and readers, which recognize and bind to m^6A-modified RNA [11]. Among them, YTHDF2, an m^6A reader, promotes gastric cancer drug resistance in an m^6A-dependent manner by recruiting the lncRNA CBSLR [11]. FTO can regulate the expression of LINC00022, which promotes cell proliferation and tumor growth in esophageal squamous cell carcinoma [12]. The interaction between lncRNAs and m^6A regulators can also modulate cellular biological functions and the expression of target genes [13]. m^6A modifications of lncRNAs may also influence tumor cell malignancy, such as proliferation, migration, and invasion, by affecting RNA structure and function in cancer [9, 14, 15]. For example, the lncRNA BLACAT3 is upregulated in bladder cancer, and m^6A modification stabilizes its structure, promoting angiogenesis and vascular migration [16]. m6A-modified FAM83H-AS1 preferentially regulates PTBP1 in colorectal cancer, promoting CRC progression through RNA splicing [17]. Upregulation of m^6A-modified SNHG17 exacerbated the malignant phenotype of gefitinib-resistant lung adenocarcinoma (LUAD) cells [18]. However, only a few reports have described the correlation between the m^6A modification of lncRNAs and PaCa. Thus, we need to construct an m^6A-related lncRNA prognostic model for PaCa that can serve as a powerful clinical feature for predicting prognosis and responsiveness to immunotherapy.

Materials and methods

Source of datasets and the m^6A-related prognostic signature as a risk model in PaCa patients

RNA-seq data and associated phenotypic information from 178 PaCa patients were retrieved from The Cancer Genome Atlas (TCGA) database (https://portal.gdc.cancer.gov/). The annotations of the lncRNAs were obtained from the GENCODE website (https://www.gencodegenes.org). A total of 25 m^6A-related genes (writers, readers, and erasers) were included. To design the m^6A-related lncRNA prognostic signature, m^6A-related lncRNAs were selected through univariate Cox regression, LASSO regression, and multivariate Cox regression analyses to construct a novel prognostic lncRNA signature. The risk score for each sample was calculated *via* the following formula:

$$riskscore = \sum ExpLncRNA_i * \beta_i \quad (1)$$

where $ExpLncRNA_i$, i and β_i represent the lncRNA expression level, the number of characteristic lncRNA, and the coefficient index, respectively [19, 20]. The patients were divided into low-risk and high-risk groups according to the median cutoff value of the risk score. Survival curves were used to assess the ability of the m^6A-related signature to differentiate prognoses between different risk groups. Time-dependent receiver operating characteristic (ROC) curves were used to evaluate the reliability of the signature *via* the "timeROC" package. Stratified analysis was performed to assess the prognostic value of m^6A-related features across different subgroups on the basis of clinical characteristics.

Establishment and evaluation of a nomogram scoring system

We performed univariate and multivariate Cox regression analyses on the 5-gene signature and clinical indicators to identify independent prognostic factors and developed a nomogram to quantify the 1-year, 3-year, and 5-year survival probabilities of PaCa patients on the basis of these independent predictive factors. Calibration curves and decision curve analysis (DCA) were used to assess the discrimination and accuracy of the nomogram model.

Functional pathway analyses

Gene Ontology (GO) and Kyoto Encyclopedia of Genes and Genomes (KEGG) analyses were performed by the R packages "clusterProfiler," "org.Hs.eg.db," "enrichplot," and "ggplot2" (R version 4.2.1). The functional candidates were further filtered with an adjusted P value < 0.05. Additionally, gene set enrichment analysis (GSEA) was conducted by GSEA software (version 4.2.1), with v7.4 from the Molecular Signatures Database (MSigDB) used as the target gene set. The entire tumor transcriptome was used for GSEA, and only gene sets with $P < 0.05$ and FDR < 0.25 were considered statistically significant.

Immune phenotype of the m^{6}A-related prognostic signature

The abundances of 64 types of tumor-infiltrating immune cells (TIICs) in PaCa samples were calculated by the Xcell algorithm in R. Tumor purity, immune scores, stromal scores, and ESTIMATE scores were evaluated by the ESTIMATE algorithm. TME-related biomarkers were analyzed as described previously [19].

Somatic mutation analysis

The waterfall function of the "maftools" R package was used to illustrate the mutational landscape of the high-risk and low-risk groups to quantify the somatic mutation count and tumor mutation burden (TMB) for each individual patient. To identify the significant differences in somatic mutation counts and TMB levels between the high-risk and low-risk groups, we performed the Wilcoxon test. The Kaplan-Meier method was subsequently applied to compare survival rates to analyze the differences between the high-mutation and low-mutation groups, as well as between risk categories.

Prediction of therapeutic response by the m^{6}A-related lncRNA risk score

To investigate the response to immunotherapy in different risk groups, tumor immune dysfunction and exclusion (TIDE) (http://tide.dfci.harvard.edu) was utilized to est imate the immunotherapeutic effect in high- and low-risk patients, and the Wilcoxon test was applied to compare differences in TIDE-related scores between the two risk groups ($P < 0.05$). The submap algorithm (http://cloud.genepattern.org/gp) was utilized to predict the probability of response to anti-PD-1 or anti-CTLA-4 therapy in the different risk groups [21]. We obtained drug sensitivity data from two pharmacogenomic databases (PRISM and CTRP) in the online website http://www.sxdyc.com/and calculated the area under the curve (AUC) values for drug responses to evaluate the potential responses of clinical patients to candidate drugs in this study [22]. Subsequently, we calculated the Pearson correlation coefficient between the AUC values and risk scores. Pearson correlations between AUC values and risk scores were also calculated. Drugs with a negative correlations were considered beneficial for the high-risk group ($P < 0.05$). To predict the clinical performance and potential adverse effects of the drugs, ADMET analysis was conducted to assess the pharmacokinetics and in vivo safety of the candidate drugs, including absorption, distribution, metabolism, excretion, and toxicity.

Pancreatic cell lines, cell culture conditions and pancreatic tumor tissue specimens

The human PaCa cell lines PANC-1, CAPAN-1, CFPAC-1, NOPR1, SW1990 and SUIT2 were grown in DMEM supplemented with 10% fetal bovine serum, 2 mmol/L L-glutamine, 100 IU/mL penicillin G, and 100 µg/mL streptomycin. BxPC-3 and AsPC-1 cells were cultivated in RPMI 1640 in the presence of 2 mmol/L L-glutamine, 4.5 g/L glucose, 10 mmol/L HEPES, 1 mmol/L sodium pyruvate, 10% fetal bovine serum, 100 IU/mL penicillin G and 100 µg/mL streptomycin. The near-normal immortalized human hTERT-HPNE cells were grown in Medium D (InCell Corp., San Antonio, TX, USA). Medium D contained one volume of medium M3, three volumes of glucose-free DMEM, 5% FBS, 5.5 mM glucose, 10 ng/mL EGF, and 50 g/mL gentamycin. All the cell lines were routinely cultivated in a humidified 5% CO_2 atmosphere.

A total of 53 pairs of PaCa tissues and adjacent normal tissues were obtained from the Department of Surgery at Zhongshan Hospital, Fudan University (Shanghai, China). Fresh tissue samples were stored in liquid nitrogen immediately after surgical resection and stored until further use. All procedures for obtaining the tissues were conducted in accordance with ethical standards and appropriate regulatory guidelines.

RNA extraction and qRT–PCR analysis

Total RNA was extracted from the tissues by TRIzol reagent (Life Technologies, Austin, Texas, USA) according to the manufacturer's instructions (Invitrogen). RNA was quantified using a NanoDrop 2000c instrument (Thermo Fisher). Subsequently, 1 µg of total RNA was reverse transcribed into cDNA by the Prime Script RT Reagent Kit (Takara, Dalian, China) following the manufacturer's protocol. Real-time quantitative PCR (qRT-PCR) analysis was conducted using TB Green Premix Ex Taq (Takara, Dalian, China). The expression levels of each lncRNA were normalized to

18 S rRNA expression, and each sample was tested in triplicate. The relative expression of the lncRNAs was quantified by the $2^{-\Delta\Delta Ct}$ method [7]. The qRT–PCR primer sequences are provided in Table S1.

Analysis of methylation levels by the T3 DNA ligase method

The m^{6}A binding sites of the five lncRNAs were identified in the SRAMP database (http://www.cuilab.cn/sramp/) (Table S2). The m^{6}A modification level of the lncRNAs was measured by the T3 DNA ligase method, as shown in Supplemental Fig. S1. The DNA probes L1 (left) and R1 (right) were designed around the m^{6}A modification sites, with universal primers for PCR amplification and target-specific sequences that pair with RNA regions adjacent to the m^{6}A site. When m^{6}A is present, probes L1 and R1 hybridize with the flanking sequences but cannot ligate across the m^{6}A site. As a result, the ligation product is reduced, leading to diminished PCR amplification of the modified sequences, whereas nonmodified sites can be ligated and amplified. To quantify m^{6}A modification levels, probes L2 and R2 were designed for a reference site within the same transcript that does not undergo m^{6}A modification. The ligation and PCR amplification of the reference product reflect RNA expression levels, allowing accurate comparison of m^{6}A modification content by qRT-PCR between the m^{6}A-modified site and the nonmodified reference site [23]. The complete sequences are provided in Table S3. Ligation reaction mixture A (1 μL of Probe L at a concentration of 20 nM, 1 μL of Probe R at a concentration of 20 nM, 3 μL of ligase buffer) (New England Biolabs, Beijing, China) and 1 μL of RNA sample (Table S3) were incubated at 85 °C for 3 min, followed by 35 °C for 10 min; then, Ligation Reaction Mixture B (1 μL of T3 DNA ligase (New England Biolabs, Beijing, China) at a concentration of 320 U, 2 μL of ligase buffer, and 1 μL of H_2O) was added. The final volume of the ligation mixture was 10 μL. The ligation reaction mixture was subsequently incubated at 35 °C for 15 min. One microliter of the reaction mixture was transferred for real-time quantitative PCR. The PCR system included 10 μM forward primer, 10 μM reverse primer, 2x TB green (Takara, Dalian, China) and RNase-free ultrapure water, resulting in a total PCR volume of 10 μL. The prepared PCR system was run at 95 °C for 2 min, followed by 40 cycles of 95 °C for 5 s and 60 °C for 30 s.

Statistical analysis

Statistical analyses were performed by R software version 4.2.1 and GraphPad Prism version 8.0. Continuous variables were compared *via* the Wilcoxon rank-sum test and the Mann-Whitney U test, whereas Spearman's correlation analysis was used to calculate correlation coefficients. Kaplan-Meier survival curves were plotted, and survival differences were compared *via* the log-rank test.

Results

Identification of the m^{6}A-related lncRNA signature as a risk model in PaCa patients

All PaCa RNA-seq data were first downloaded from the TCGA database, and the workflow of this study is shown in Supplemental Fig. S2. A coexpression analysis of 25 m^{6}A-related genes and 16,773 lncRNAs revealed 129 m^{6}A-related lncRNAs (|Pearson R| > 0.3, $P < 0.001$) (Fig. 1A). On the basis of the correlation between m^{6}A-related lncRNAs and the survival characteristics of PaCa patients, univariate Cox analysis revealed that 35 lncRNAs were significantly associated with prognosis (Table S4). The incorporation of these variables into LASSO Cox regression analysis with minimal lambda resulted in the selection of five m^{6}A-related lncRNAs for constructing a prognostic risk model (Fig. 1B, C). A heatmap illustrating the correlation between five lncRNAs and twenty-five m^{6}A regulators revealed a strong association (Fig. 1D). PaCa patients ($n = 178$) were accurately classified into high-risk and low-risk groups based on the median risk score. The density plot revealed a substantial discriminative ability of the risk score between the high-risk and low-risk groups (Fig. 1E). The Kaplan-Meier (K-M) survival curve revealed significantly better overall survival (OS) in the low-risk group than in the high-risk group ($P < 0.001$) (Fig. 1F). To assess the accuracy of the prognostic risk model in predicting 1-year, 3-year, and 5-year OS, area under the ROC curve (AUC) values of 0.699, 0.783, and 0.871, respectively, were generated (Fig. 1G).

Validation of the expression of five m^{6}A-related lncRNAs and m^{6}A modification levels in PaCa cell lines and tumor tissues

Next, we used qRT-PCR to measure the expression levels of these five m^{6}A-related lncRNAs in 53 pairs of PaCa and adjacent normal tissues, as well as across eight cell lines. Our findings indicate that, at the cellular level, the expression of these five lncRNAs is upregulated in most PaCa cell lines (Fig. 2A-E). At the tissue level, the expression levels of LINC01091, AC092171.5, AC015660.1, and AC005332.6 were greater in PaCa tissues than in adjacent normal tissues, whereas the expression level of AC096733.2 was not different from that in adjacent normal tissues (Fig. 2F-J). We further analyzed the m^{6}A modification levels of the five

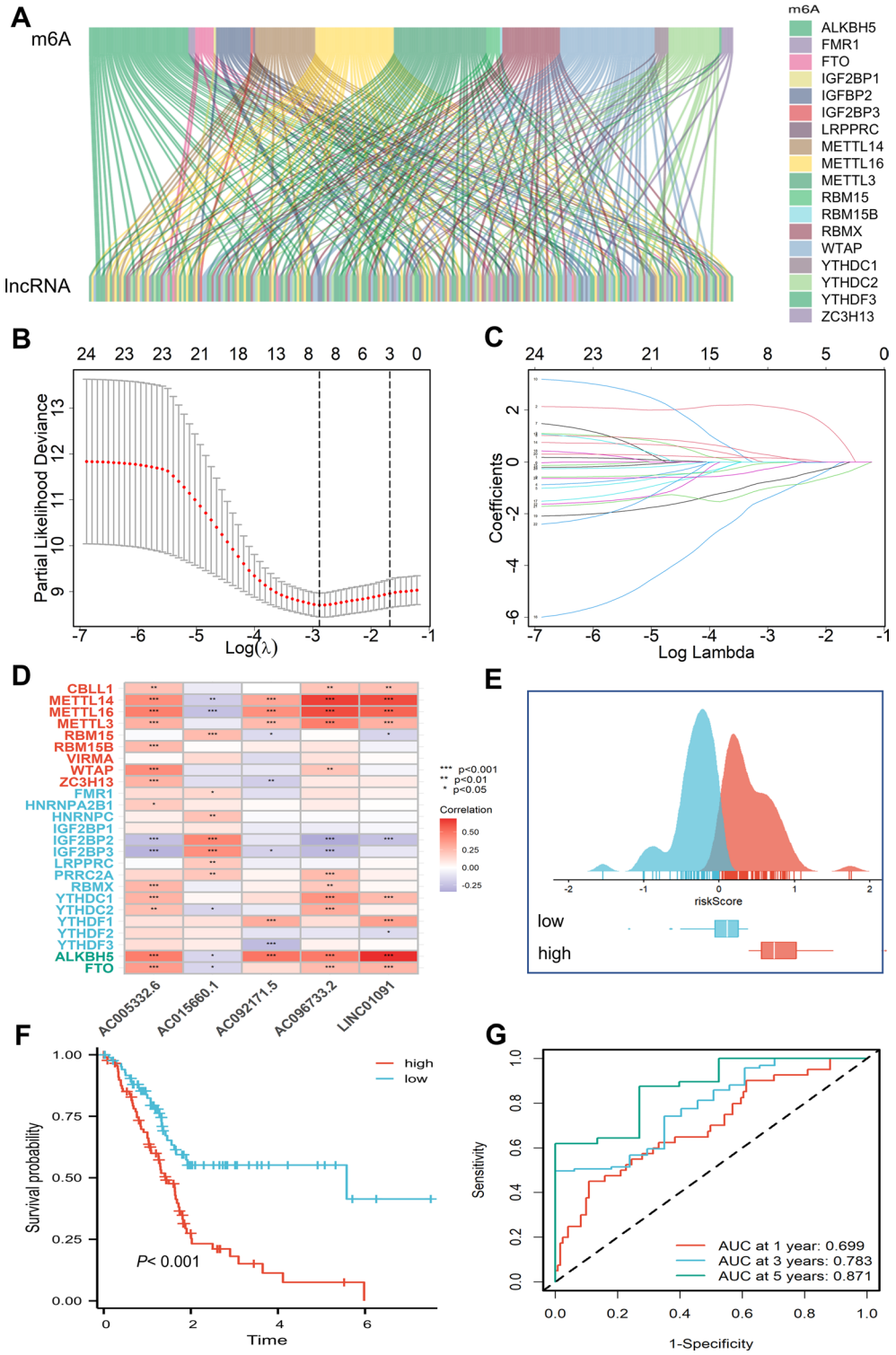

Fig. 1 Construction and validation of the m^{6}A-related lncRNA network and prognostic risk model for PaCa. **A**) Sankey diagram demonstrating the coexpression relationships between 25 m^{6}A genes and m^{6}A-related lncRNAs. **B**) Cross-validation method for selecting optimal lncRNAs. **C**) Lasso coefficient curve. **D**) Heatmap displaying the correlation between 5 lncRNAs and m^{6}A-related genes. **E**) Density distribution plots for the two risk groups. **F**) K–M survival curves for OS between the high-risk and low-risk groups in the TCGA-PaCa cohort. **G**) AUC values of the prognostic risk model for different time periods. *P* values are shown as follows: ns, not significant; $*P<0.05$; $**P<0.01$; $***P<0.001$

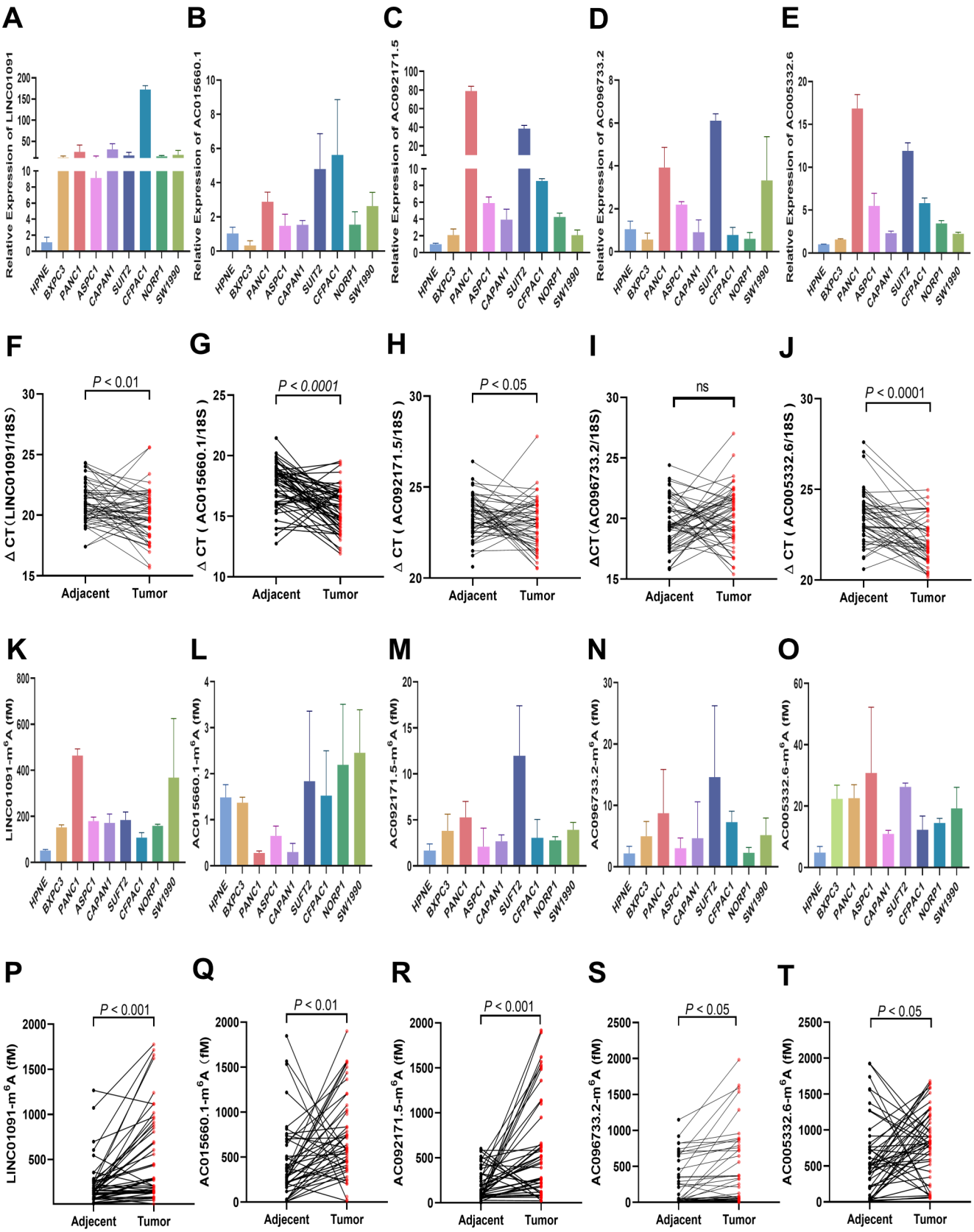

Fig. 2 Analyses of the expression and m6A modification levels of 5 m6A-related lncRNAs (LINC01091, AC015660.1, AC092171.5, AC096733.2, and AC005332.6) in pancreatic cells and tumor tissues. **A-J**) The expression levels of 5 m6A-related lncRNAs in cell lines (**A-E**) and PaCa tissue (**F-J**). **K-T**) The m^6A modification levels of 5 m^6A-related lncRNAs in cell lines (**K-O**) and PaCa tissue (**P-T**). *P* values are shown as follows: ns, not significant; $*P < 0.05$; $**P < 0.01$; $***P < 0.001$.

lncRNAs at both the cellular and tissue levels and found that the m^{6}A modification levels of four lncRNAs (LINC01091, AC096733.2, AC092171.5 and AC005332.6) in all seven PaCa cell lines (PANC-1, BxPC-3, AsPC-1, CAPAN1, SUIT2, CFPAC1 and SW1990) were greater than those observed in the HPNE cells (Fig. 2K-O). We also found that the m^{6}A modification levels of all five lncRNAs were elevated in PaCa tumor tissue compared with normal control tissue (Fig. 2P-T). In conclusion, these findings demonstrate the stability of the risk model in predicting the prognosis of PaCa patients.

Stratified survival analysis and evaluation of the prognostic model in the PaCa cohort

The clinical phenotypic information of PaCa patients was initially obtained from TCGA-PaCa. To further validate the prognostic value of the risk model across subgroups with different clinical characteristics, a stratified analysis was conducted. Patients were divided into subgroups on the basis of sex, age, grade, pathological stage, and TNM stage, followed by survival analysis. The risk score derived from this predictive model was significantly positively correlated with both the pathological stage and the T stage according to the TNM classification (Fig. 3A). The proportion of high-risk patients was significantly greater than that of low-risk patients (Fig. 3B). The K–M survival curves demonstrated that, with the exception of Stage III-IV patients, the low-risk group presented better clinical outcomes across all subgroups (Fig. 3C-J). Furthermore, univariate and multivariate Cox analyses were performed for key clinicopathological factors and genetic characteristics. In the univariate analysis, the hazard ratio (HR) for the risk score was 1.476, with a 95% confidence interval (CI) of 1.319–1.552 ($P < 0.001$). In the multivariate analysis, the hazard ratio (HR) was 1.479, with a 95% CI of 1.312–1.557 ($P < 0.001$), indicating that the m^{6}A-related lncRNA risk score is an independent prognostic risk factor (Table S5 and Table S6). The concordance index (C-index) was calculated to evaluate the specificity and sensitivity of the risk score in predicting PaCa patient prognosis. These findings suggest that the C-index of the risk score was greater than those of clinical parameters (Supplemental Fig. S3A). Similarly, the AUC for the risk score (AUC = 0.871) was greater than that for age (AUC = 0.614), sex (AUC = 0.441), grade (AUC = 0.539), and stage (AUC = 0.633), underscoring the high reliability of the m^{6}A-related lncRNA risk model in predicting the prognosis of PaCa patients (Supplemental Fig. S3B). On the basis of independent prognostic factors, a comprehensive nomogram was developed to quantitatively predict the 1-year, 3-year, and 5-year OS probabilities of PaCa patients (Supplemental Fig. S3C). The calibration curves revealed a high degree of concordance between the predicted OS and the actual OS (Supplemental Fig. S3D). Decision curve analysis (DCA) was used to assess the clinical applicability of the nomogram. Compared with models based solely on clinical features, the comprehensive nomogram yielded greater net benefit, potentially contributing to improved clinical management (Supplemental Fig. S3E).

Identification of the immune landscape between the high-risk and low-risk groups in PaCa

An increasing number of studies have shown that tumor cell-induced abnormalities in the TME can interfere with immune cell functions [24]. On the basis of the differentially expressed genes (DEGs) between the high-risk and low-risk PaCa groups (Table S7), GO and KEGG analyses revealed that a series of immune-related biological processes, such as the B-cell receptor complex and the immunoglobulin complex, were involved in PaCa progression (Fig. 4A). GSEA was also performed on the DEGs to identify the biological processes associated with the two risk groups (Fig. 4B, C). We demonstrated that the low-risk group was enriched primarily in immune-related processes, such as the B-cell receptor signaling pathway, the MAPK cascade, and the Wnt signaling pathway, whereas the high-risk group was enriched in cancer-related processes, such as focal adhesion and ECM-receptor interactions. Additionally, we observed significant changes in the infiltration of immune cell types, with most adaptive immune cells being more abundant in the low-risk group (Supplemental Fig. S4). Because TME-related signaling pathways were enriched through functional enrichment analysis, we also explored the relationships between the risk score and TME characteristics. The ESTIMATE and CIBERSORT algorithms were used to analyze the tumor microenvironment. The stromal score of PaCa patients in the high-risk group was greater than that of patients in the low-risk group, and the risk score was highly positively correlated with the stromal score (Fig. 4D, E). We further investigated the relationships between the risk score and TME components. Our findings indicated that the risk score was significantly positively correlated with the expression of most ECM-collagen features (Supplemental Fig. S5). We subsequently analyzed the correlations between the five m^{6}A-related lncRNAs in the prognostic model and different immune cell types, and the results revealed significant correlations with most immune cells (Fig. 4F). The five m6A-related lncRNAs also showed significant associations with human leukocyte antigen (HLA) and major histocompatibility complex (MHC) molecules (Fig. 4G, H), suggesting their potential predictive value in assessing the tumor immune microenvironment and immune response.

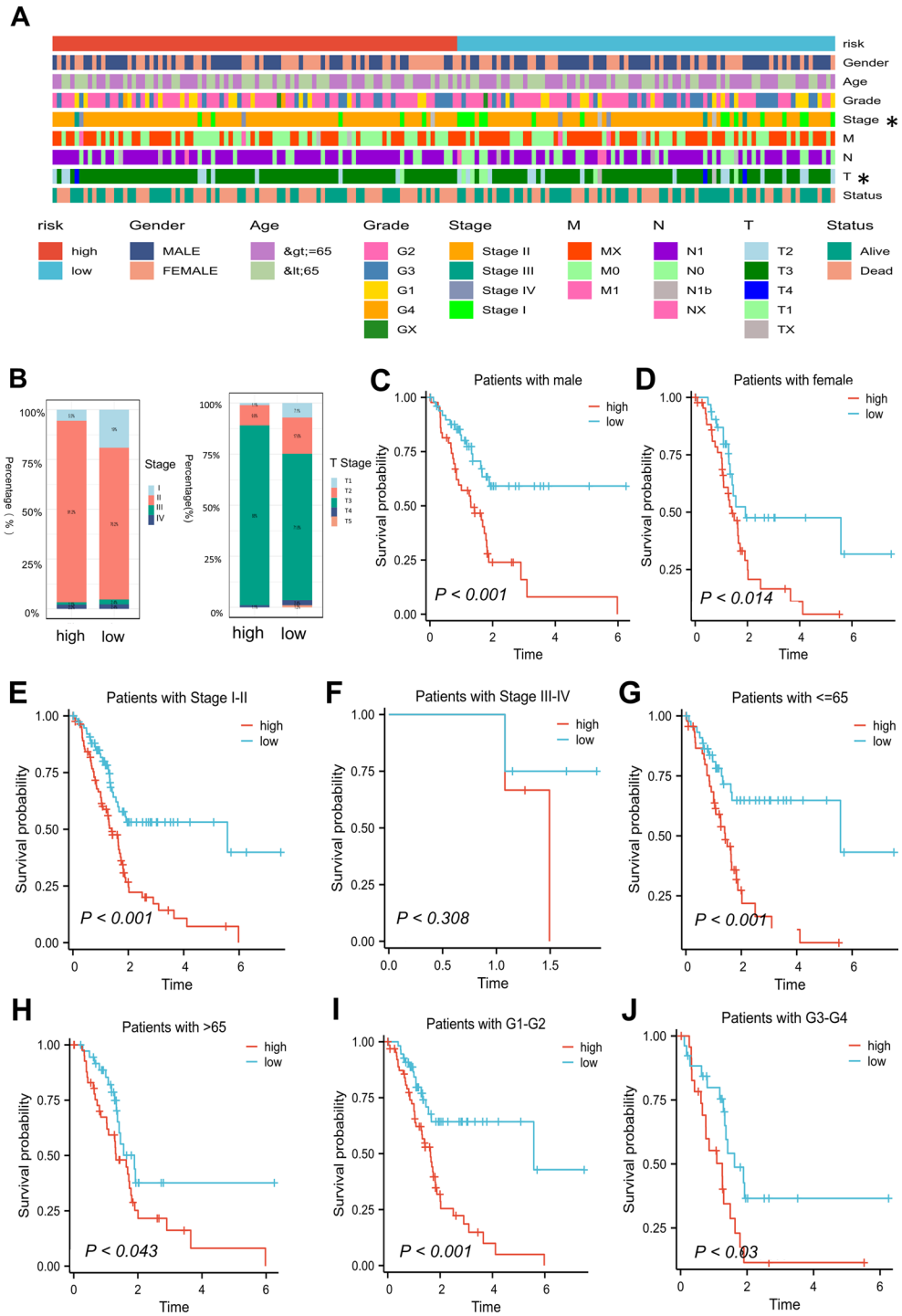

Fig. 3 Stratified survival analysis and visualization of the clinical characteristics of PaCa patients based on risk score. **A**, **B**) The risk score was significantly associated with the stage and topography of patients in the TCGA-PaCa cohort. **C**-**J**) **K**–**M** survival curves for OS in the two risk groups. (Gender, Stage, Age and Grade). *P* values are shown as follows: ns, not significant; $*P<0.05$; $**P<0.01$; $***P<0.001$

Abnormal genomic variation in different subgroups based on the m^{6}A-related prognostic risk model of PaCa

To explore the relationship between PaCa development and genetic mutations, mutation frequencies were calculated separately for the high-risk and low-risk groups, and the associations between the risk score and mutational landscape were analyzed. The top 20 most frequently mutated genes in the high-risk and low-risk groups, namely TP53, KRAS, SMAD4, CDKN2A, TTN, MUC16, RNF43, TNXB, HECW2, RYR1, TGFBR2, ARID1A, TPO, GLI3, PCDH15, LRP1B, RNF213, RIMS2, CACNA1B, and GNAS, are shown in Fig. 5A and B. Moreover, the TP53 and KRAS mutation rates were significantly greater in the high-risk group (Fig. 5C), which indicated that the TMB

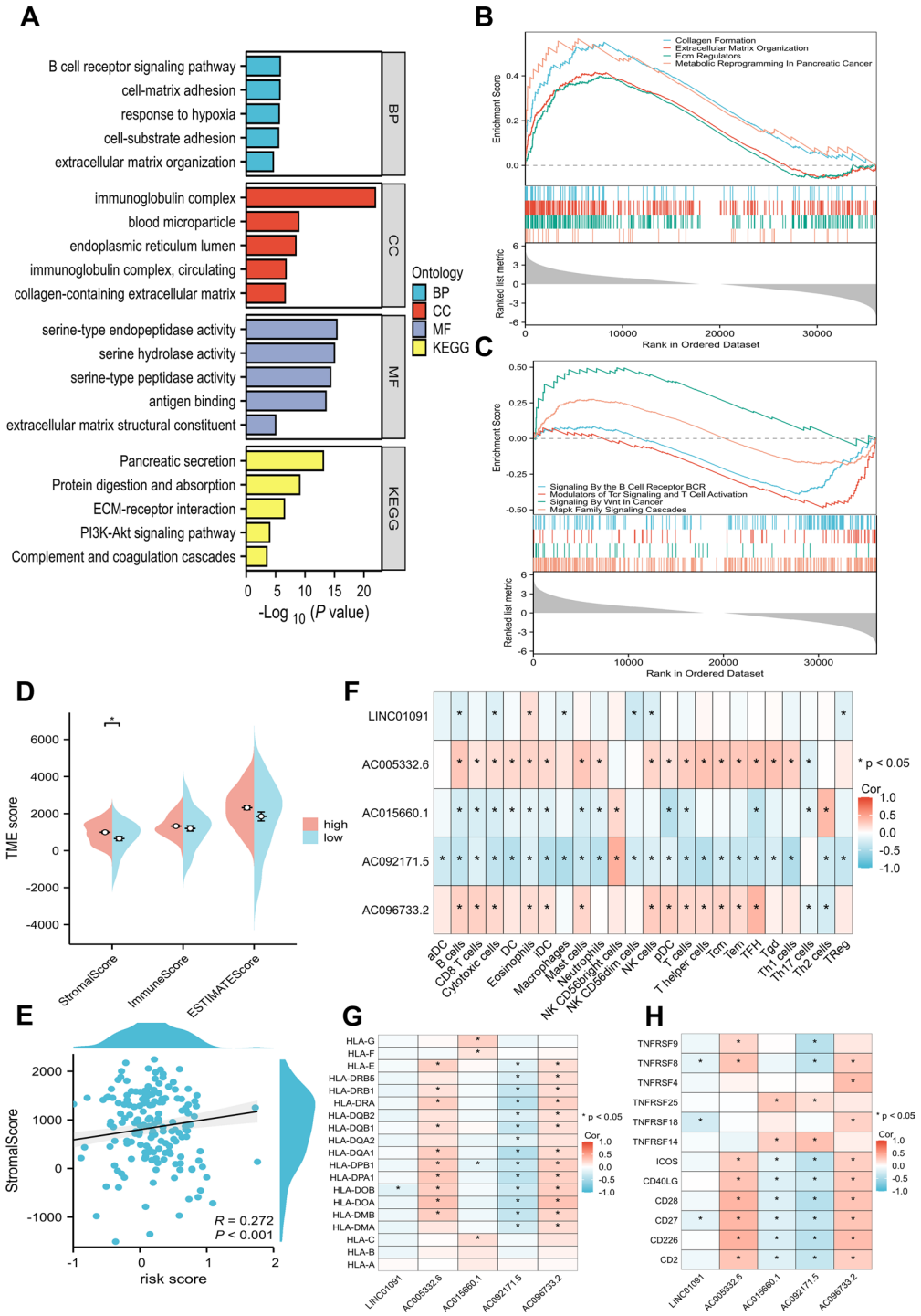

Fig. 4 Immune landscape in high- and low-risk groups of PaCa patients. **A**) Bar plot of the results of the GO and KEGG enrichment analyses. **B**, **C**) GSEA of the DEGs in the high-risk groups (**B**) and the low-risk groups (**C**). **D**) Comparisons of the stromal, immune and ESTIMATE scores between the two risk groups. **E**) Association between the stromal score and the risk score. **F**) The risk score was correlated with immune cell infiltration. **G**, **H**) The risk score correlated with the HLA (**G**) and MHC (**H**) gene sets between the two risk groups. *P* values are shown as follows: ns, not significant; $*P<0.05$; $**P<0.01$; $***P<0.001$

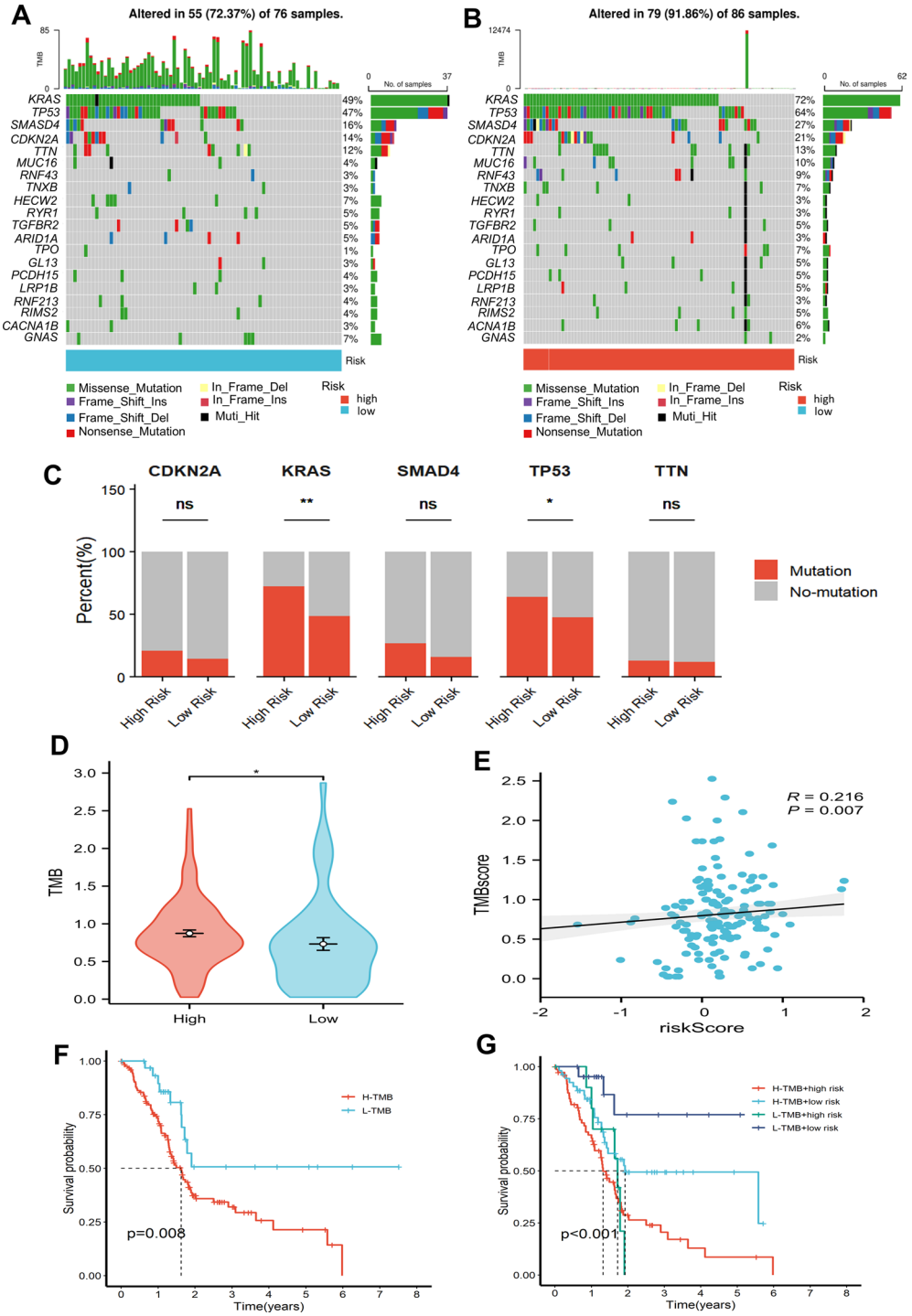

Fig. 5 Mutation status in the two risk groups in PaCa. **A**, **B**) The 20 most frequently mutated genes in the low-risk (**A**) and high-risk groups (**B**). **C**) Mutation rates of the top five mutant genes in the two risk groups. **D**) TMB in the high-risk and low-risk groups. **E**) Correlation between the risk score and TMB score in PaCa patients. **F**) Effect of the risk score on the prognosis of patients with different TMB levels. **G**) Relationships between the prognosis of patients with PaCa and TMB. *P* values are shown as follows: ns, not significant; $*P<0.05$; $**P<0.01$; $***P<0.001$

was significantly greater in the high-risk group than in the low-risk group. We also demonstrated that the risk score was positively correlated with TMB in PaCa patients (Fig. 5D, E) and that patients with high TMB in the high-risk group had significantly worse OS (Fig. 5F, G). Our results suggest that the combination of the risk score and TMB may serve as a valuable biomarker for predicting the prognosis of PaCa patients, which provides a comprehensive view of the mutational landscape in relation to the risk levels and survival outcomes of PaCa patients.

Sensitivity of high-risk populations of PaCa patients to immunotherapy and candidate drugs

A lower TIDE score indicates a lower probability of immune evasion, suggesting a greater likelihood of benefiting from immunotherapy. Our results revealed that the low-risk group had significantly lower TIDE scores ($P < 0.001$). Moreover, the T-cell exclusion score was lower in the low-risk group ($P < 0.01$), indicating a potential increased sensitivity to immunotherapy in these patients (Fig. 6A). Submap analysis revealed that low-risk PaCa patients exhibited a more promising response to PD-1 blockade therapy (Bonferroni-corrected $P = 0.008$), further suggesting that individuals in the low-risk group are more likely to benefit from anti-PD-1 checkpoint inhibitor treatment (Fig. 6B). Furthermore, drug sensitivity was assessed the drug response data derived from CTRP and PRISM for different risk groups. Initially, 113 drugs or compounds were identified at the intersection of CTRP and PRISM (Table S8). Subsequent differential drug response analysis identified significantly distinct drugs, selecting only those with lower AUC values in the high-risk group, which corresponded to increased treatment sensitivity. A lower dose-response AUC value corresponds to greater sensitivity to treatment. Additionally, drugs with a negative correlation between AUC values and risk scores were identified. Ultimately, three drugs or compounds, WZ8040, selumetinib, and bortezomib, were found to have substantial therapeutic potential in high-risk patients, as evidenced by lower estimated AUC values and a negative correlation with the risk score (Fig. 6C). To further assess the therapeutic potential of these candidate drugs, ADMET analysis was performed in the ADMETlab 2.0 database (https://admetmesh.scbdd.com/). We found that selumetinib was the most promising drug, followed by WZ8040 and bortezomib (Fig. 6D).

Discussion

To better understand the potential roles of m^{6}A-related lncRNAs in PaCa, we first developed a signature of five m^{6}A-related lncRNAs (LINC01091, AC096733.2, AC092171.5, AC015660.1, and AC005332.6) by LASSO regression and Cox analyses to predict the prognosis of PaCa patients. Our results demonstrated that these m^{6}A-related lncRNAs may be independent prognostic variables for PaCa and may successfully stratify PaCa patients into two distinct prognostic categories. We next investigated whether the signature of five m^{6}A-related lncRNAs exhibited high accuracy in prognosis prediction by analyzing receiver operating characteristic curves and calibration curves and established a nomogram incorporating clinical parameters and risk ratings to increase the predictive potential of the five m^{6}A-related lncRNA signatures. Among them, LINC01091 is highly expressed and enhances the proliferation, migration, and invasion of gastric cancer cells through the microRNA-128-3p/ELF4/CDX2 axis [25]. AC092171.5 is associated with poor prognosis in patients with lung adenocarcinoma [26]. AC005332.6 is highly expressed in PaCa and is a copper-dependent cell death-related lncRNA that plays a role in the construction of a cuproptosis-related model. AC005332.6 has been identified as an independent prognostic variable in PaCa and has high accuracy in prognosis prediction [27].

The tumor microenvironment consists of noncancerous stromal cells, soluble growth factors, cytokines, proteases, cancer cells, and the extracellular matrix (ECM), which provides essential signals for tumor survival, growth, and invasion while also impeding antitumor immunity [28]. ECM accumulation is a hallmark of tumors, and in various cancer types, a higher ECM content is associated with a poorer prognosis [19, 29]. We further explored the potential associations of these five m^{6}A-related lncRNAs with individual immune infiltration, mutation, immunotherapy response, and drug sensitivity in PaCa. Our previous study also indicated that lncRNAs, as prognostic biomarkers, play critical roles in immune regulation and the TME of PaCa [30]. Here, we found that the high-risk group was predominantly enriched in the ECM and focal adhesion pathways, whereas the low-risk group was enriched primarily in the T-cell and B-cell receptor signaling pathways, which indicated that the risk score was positively correlated with ECM characteristics and suggested that a higher risk score might be associated with increased ECM accumulation. Additionally, the risk score was positively correlated with the stromal score, which might represent a greater degree of stromal cell infiltration in the TME of the high-risk group. Immune cells play crucial roles in the TME, and the success of tumor immunotherapy relies on a comprehensive understanding of

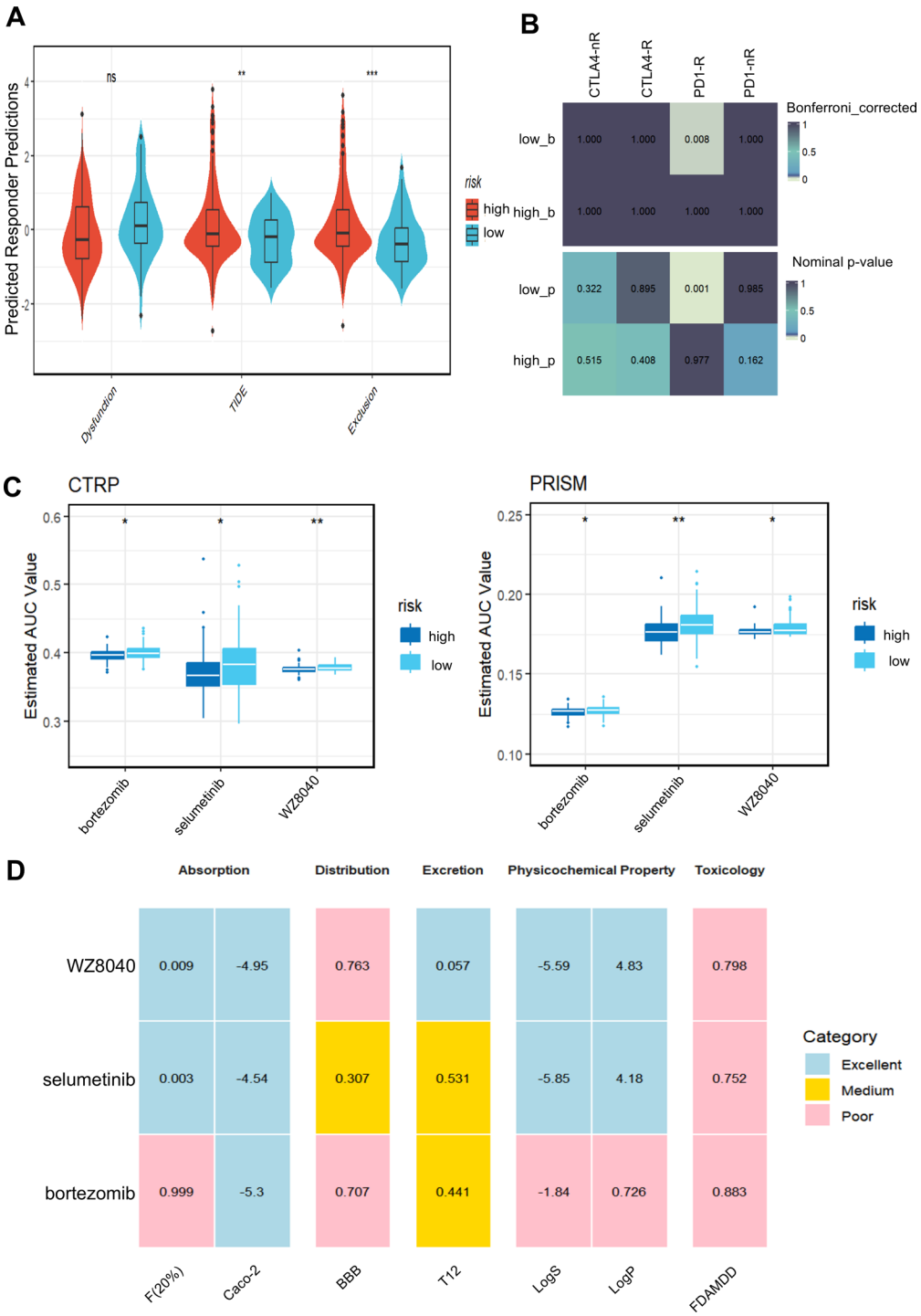

Fig. 6 Identification of potential therapeutic drugs for PaCa patients with high risk scores. **A**) TIDE score in the high-risk and low-risk groups. **B**) Sensitivity of different subgroups to immunotherapy. **C**) Different drug response assessments of potential therapeutic drugs in the CTRP and PRISM databases. **D**) ADMET attributes of potential therapeutic drugs. $*P<0.05$; $**P<0.01$; $***P<0.001$

the TME and immune evasion mechanisms. In this complex network, tumor cells, the stroma, and infiltrating immune cells work together in a coordinated manner [31]. HLA and MHC molecules are responsible for antigen presentation in immune responses, which determines whether the immune system can recognize and eliminate tumor cells. MHC class I molecules present antigens to $CD8^+$ T cells, activating them to attack tumors, whereas MHC class II molecules, which are expressed on dendritic cells and other antigen-presenting cells, present antigens to $CD4^+$ T cells, coordinating the

immune response [29]. Tumors evade immune surveillance by downregulating MHC class I molecules or altering HLA molecules [32, 33]. Therefore, understanding the role of HLA/MHC molecules in the TME and how tumors exploit alterations in these molecules to achieve immune evasion is crucial for developing effective immunotherapy strategies. Our findings demonstrated that immune cells, such as $CD8^+$ T cells, $CD4^+$ T cells, and NK cells, were significantly different between the high- and low-risk groups, with these cells predominantly enriched in the low-risk group. The significant correlation between m6A-related lncRNAs and HLA/MHC molecules suggests their potential predictive value in evaluating the TME and immune response.

Finally, we demonstrate that the model has the potential to be applied in personalized treatment plans for PaCa patients, particularly in the context of immunotherapy. The TMB is associated with the formation of neoantigens, which can activate antitumor immunity, making it a reliable biomarker for predicting responses to PD-L1 therapy [34]. Although a higher TMB is typically correlated with better responses to immunotherapy, the high-risk group had a higher TMB than the low-risk group did in our study, which may indicate that immune evasion mechanisms or an immunosuppressive TME enables resistance to immune attacks, leading to a poorer prognosis.

The identification of monoclonal antibodies that target immune checkpoint molecules has led to significant breakthroughs in cancer treatment. Inhibitors of PD-1/PD-L1 and CTLA-4 have shown promising therapeutic outcomes [35]. In our study, submap analysis revealed that the low-risk group demonstrated a significantly greater response rate to PD-L1 immunotherapy than did the high-risk group [21]. Additionally, the risk score may aid in screening therapeutic drugs. Although gemcitabine is the first-line treatment for PaCa, most patients eventually develop resistance to it [36]. Drug repurposing, which involves investigating existing drugs for new therapeutic targets, has made significant strides in cancer drug development [37, 38]. Our study revealed that candidate drugs (WZ8040, selumetinib, and bortezomib) from two pharmacogenomic databases were associated with greater therapeutic sensitivity in the high-risk group. Therefore, PaCa patients in both high- and low-risk groups are more likely to benefit from effective treatment when receiving appropriate immunotherapeutic drugs. The establishment of an m6A-related lncRNA model provides a new strategy for improving the clinical prognosis of PaCa patients.

In summary, we established a prognostic risk model for PaCa patients that includes LINC01091, AC096733.2, AC092171.5, AC015660.1 and AC005332.6. We found that the risk score was strongly associated with the TME and immune cell infiltration in high-risk PaCa patients who are more sensitive to WZ8040, selumetinib and bortezomib, which demonstrates that our m^{6}A-related risk model may serve as a reliable prognostic biomarker for personalized PaCa patients.

Supplementary Information The online version contains supplementary material available at https://doi.org/10.1007/s00018-024-05573-w.

Author contributions Jin Wang: Investigation, Funding acquisition, Writing-review & editing. Zhihui Bai: Data curation, Formal analysis, Writing-original draft. Qianlin Xia: Data curation, Formal analysis. Wanli Xu: Data curation, Validation. Zhirong Wu: Clinic samples collection. Xiaomeng He: Cell culture, Data curation. Xin Zhang and Mengting Luo: Resources. Zhefeng Wang and Huaqin Sun: Data Analysis. Songmei Liu: Conceptualization.

Funding This research was supported by a grant from the Natural Science Foundation of Fujian Province (2024J011432), China, a grant from the Science and Technology Development Fund of the Pudong New Area (PKJ2021-Y53), China, and a grant from The Science and Technology Plan Project of Xiamen (3502Z20224012).

Data availability The data analyzed are available from the corresponding author on reasonable request.

Declarations

Ethics approval and consent to participate All human specimens were collected in accordance with the protocol approved by the Ethics Committees of Zhongshan Hospital (Xiamen) of Fudan University (B2024-018) and all the study subjects provided written informed consent to participate.

Consent for publication Not applicable.

Competing interests The authors have no financial interest.

References

1. Sung H, Ferlay J, Siegel RL, Laversanne M, Soerjomataram I, Jemal A, Bray F (2021) Global Cancer statistics 2020: GLOBOCAN estimates of incidence and Mortality Worldwide for 36

cancers in 185 countries. Cancer J Clin 71(3):209–249. https://doi.org/10.3322/caac.21660
2. Kamisawa T, Wood LD, Itoi T, Takaori K (2016) Pancreatic cancer. Lancet (London England) 388(10039):73–85. https://doi.org/10.1016/S0140-6736(16)00141-0
3. Sun H, Ma H, Hong G, Sun H, Wang J (2014) Survival improvement in patients with pancreatic cancer by decade: a period analysis of the SEER database, 1981–2010. Sci Rep 4:6747. https://doi.org/10.1038/srep06747
4. Siegel RL, Miller KD, Jemal A (2019) Cancer statistics, 2019. Cancer J Clin 69(1). https://doi.org/10.3322/caac.21551
5. Peng WX, Koirala P, Mo YY (2017) LncRNA-mediated regulation of cell signaling in cancer. Oncogene 36(41):5661–5667. https://doi.org/10.1038/onc.2017.184
6. Yang X, Liu M, Li M, Zhang S, Hiju H, Sun J, Mao Z, Zheng M, Feng B (2020) Epigenetic modulations of noncoding RNA: a novel dimension of Cancer biology. Mol Cancer 19(1):64. https://doi.org/10.1186/s12943-020-01159-9
7. He X, Chen L, Di Y, Li W, Zhang X, Bai Z, Wang Z, Liu S, Corpe C, Wang J (2024) Plasma-derived exosomal long noncoding RNAs of pancreatic cancer patients as novel blood-based biomarkers of disease. BMC Cancer 24(1):961. https://doi.org/10.1186/s12885-024-12755-z
8. Ma Y, Di Y, Li Q, Zhan Q, He X, Liu S, Zou H, Corpe C, Chen L, Wang J (2022) LncRNAs as epigenetic regulators of epithelial to mesenchymal transition in pancreatic cancer. Discov Oncol 13(1):61. https://doi.org/10.1007/s12672-022-00522-0
9. Liu S, Di Y, Li Q, Chen L, Ma Y, He X, Corpe C, Zhang X, Xu J, Wang J (2023) Exosomal lncRNA LINC01268 promotes pancreatic cancer progression via the miR-217-KIF2A-PI3K/AKT axis. Genes Dis 10(5):1799–1801. https://doi.org/10.1016/j.gendis.2022.12.018
10. Desrosiers R, Friderici K, Rottman F (1974) Identification of methylated nucleosides in messenger RNA from Novikoff hepatoma cells. Proc Natl Acad Sci USA 71(10):3971–3975
11. Yang H, Hu Y, Weng M, Liu X, Wan P, Hu Y, Ma M, Zhang Y, Xia H, Lv K (2022) Hypoxia inducible lncRNA-CBSLR modulates ferroptosis through m6A-YTHDF2-dependent modulation of CBS in gastric cancer. J Adv Res 37. https://doi.org/10.1016/j.jare.2021.10.001
12. Cui Y, Zhang C, Ma S, Li Z, Wang W, Li Y, Ma Y, Fang J, Wang Y, Cao W et al (2021) RNA m6A demethylase FTO-mediated epigenetic up-regulation of LINC00022 promotes tumorigenesis in esophageal squamous cell carcinoma. J Experimental Clin Cancer Research: CR 40(1):294. https://doi.org/10.1186/s13046-021-02096-1
13. Ma S, Chen C, Ji X, Liu J, Zhou Q, Wang G, Yuan W, Kan Q, Sun Z (2019) The interplay between m6A RNA methylation and noncoding RNA in cancer. J Hematol Oncol 12(1):121. https://doi.org/10.1186/s13045-019-0805-7
14. Li J, Zhang H, Wang H (2022) N1-methyladenosine modification in cancer biology: current status and future perspectives. Comput Struct Biotechnol J 20:6578–6585. https://doi.org/10.1016/j.csbj.2022.11.045
15. Qin S, Mao Y, Wang H, Duan Y, Zhao L (2021) The interplay between m6A modification and non-coding RNA in cancer stemness modulation: mechanisms, signaling pathways, and clinical implications. Int J Biol Sci 17(11):2718–2736. https://doi.org/10.7150/ijbs.60641
16. Xie J, Zhang H, Wang K, Ni J, Ma X, Khoury CJ, Prifti V, Hoard B, Cerenzia EG, Yin L et al (2023) M6A-mediated-upregulation of lncRNA BLACAT3 promotes bladder cancer angiogenesis and hematogenous metastasis through YBX3 nuclear shuttling and enhancing NCF2 transcription. Oncogene 42(40):2956–2970. https://doi.org/10.1038/s41388-023-02814-3
17. Luo X-J, Lu Y-X, Wang Y, Huang R, Liu J, Jin Y, Liu Z-K, Liu Z-X, Huang Q-T, Pu H-Y et al (2024) M6A-modified lncRNA FAM83H-AS1 promotes colorectal cancer progression through PTBP1. Cancer Lett 598217085. https://doi.org/10.1016/j.canlet.2024.217085
18. Zhang H, Wang S-Q, Wang L, Lin H, Zhu J-B, Chen R, Li L-F, Cheng Y-D, Duan C-J, Zhang C-F (2022) m6A methyltransferase METTL3-induced lncRNA SNHG17 promotes lung adenocarcinoma gefitinib resistance by epigenetically repressing LATS2 expression. Cell Death Dis 13(7):657. https://doi.org/10.1038/s41419-022-05050-x
19. Chang J, Wu H, Wu J, Liu M, Zhang W, Hu Y, Zhang X, Xu J, Li L, Yu P et al (2023) Constructing a novel mitochondrial-related gene signature for evaluating the tumor immune microenvironment and predicting survival in stomach adenocarcinoma. J Translational Med 21(1):191. https://doi.org/10.1186/s12967-023-04033-6
20. Cui H, Ren X, Dai L, Chang L, Liu D, Zhai Z, Kang H, Ma X (2023) Comprehensive analysis of nicotinamide metabolism-related signature for predicting prognosis and immunotherapy response in breast cancer. Front Immunol 14:1145552. https://doi.org/10.3389/fimmu.2023.1145552
21. Roh W, Chen P-L, Reuben A, Spencer CN, Prieto PA, Miller JP, Gopalakrishnan V, Wang F, Cooper ZA, Reddy SM et al (2017) Integrated molecular analysis of tumor biopsies on sequential CTLA-4 and PD-1 blockade reveals markers of response and resistance. Sci Transl Med 9(379). https://doi.org/10.1126/scitranslmed.aah3560
22. Guo S, Liu Y, Sun Y, Zhou H, Gao Y, Wang P, Zhi H, Zhang Y, Gan J, Ning S (2024) Metabolic-related gene Prognostic Index for Predicting Prognosis, Immunotherapy Response, and candidate drugs in Ovarian Cancer. J Chem Inf Model 64(3):1066–1080. https://doi.org/10.1021/acs.jcim.3c01473
23. Liu W, Yan J, Zhang Z, Pian H, Liu C, Li Z (2018) Identification of a selective DNA ligase for accurate recognition and ultrasensitive quantification of N(6)-methyladenosine in RNA at one-nucleotide resolution. Chem Sci 9(13):3354–3359. https://doi.org/10.1039/c7sc05233b
24. Pitt JM, Marabelle A, Eggermont A, Soria JC, Kroemer G, Zitvogel L (2016) Targeting the tumor microenvironment: removing obstruction to anticancer immune responses and immunotherapy. Annals Oncology: Official J Eur Soc Med Oncol 27(8):1482–1492. https://doi.org/10.1093/annonc/mdw168
25. Wang Q, Zhang C, Cao S, Zhao H, Jiang R, Li Y (2023) Tumor-derived exosomes orchestrate the microRNA-128-3p/ELF4/CDX2 axis to facilitate the growth and metastasis of gastric cancer via delivery of LINC01091. Cell Biol Toxicol 39(2):519–536. https://doi.org/10.1007/s10565-022-09728-y
26. Guo Y, Qu Z, Li D, Bai F, Xing J, Ding Q, Zhou J, Yao L, Xu Q (2021) Identification of a prognostic ferroptosis-related lncRNA signature in the tumor microenvironment of lung adenocarcinoma. Cell Death Discovery 7(1):190. https://doi.org/10.1038/s41420-021-00576-z
27. Chi H, Peng G, Wang R, Yang F, Xie X, Zhang J, Xu K, Gu T, Yang X, Tian G (2022) Cuprotosis programmed-cell-death-related lncRNA signature predicts prognosis and Immune Landscape in PAAD patients. Cells 11(21). https://doi.org/10.3390/cells11213436
28. Labani-Motlagh A, Ashja-Mahdavi M, Loskog A (2020) The Tumor Microenvironment: a Milieu Hindering and Obstructing Antitumor Immune responses. Front Immunol 11:940. https://doi.org/10.3389/fimmu.2020.00940
29. Izzi V, Davis MN, Naba A (2020) Pan-cancer Analysis of the genomic alterations and mutations of the Matrisome. Cancers 12(8). https://doi.org/10.3390/cancers12082046

30. Ma Y, He X, Di Y, Liu S, Zhan Q, Bai Z, Qiu T, Corpe C, Wang J (2022) Identification of prognostic immune-related lncRNAs in pancreatic cancer. Front Immunol 13:1005695. https://doi.org/10.3389/fimmu.2022.1005695
31. Locy H, de Mey S, de Mey W, De Ridder M, Thielemans K, Maenhout SK (2018) Immunomodulation of the Tumor Microenvironment: turn foe into friend. Front Immunol 9:2909. https://doi.org/10.3389/fimmu.2018.02909
32. Wieczorek M, Abualrous ET, Sticht J, Álvaro-Benito M, Stolzenberg S, Noé F, Freund C (2017) Major histocompatibility complex (MHC) class I and MHC class II proteins: conformational plasticity in Antigen Presentation. Front Immunol 8292. https://doi.org/10.3389/fimmu.2017.00292
33. Lenz TL (2024) HLA genes: a Hallmark of Functional Genetic Variation and Complex Evolution. Methods Mol Biology (Clifton NJ) 2809. https://doi.org/10.1007/978-1-0716-3874-3_1
34. Xu F, Huang X, Li Y, Chen Y, Lin L (2021) m6A-related lncRNAs are potential biomarkers for predicting prognoses and immune responses in patients with LUAD. Mol Therapy Nucleic Acids 24:780–791. https://doi.org/10.1016/j.omtn.2021.04.003
35. Rotte A (2019) Combination of CTLA-4 and PD-1 blockers for treatment of cancer. J Experimental Clin Cancer Research: CR 38(1):255. https://doi.org/10.1186/s13046-019-1259-z
36. Qi R, Bai Y, Li K, Liu N, Xu Y, Dal E, Wang Y, Lin R, Wang H, Liu Z et al (2023) Cancer-associated fibroblasts suppress ferroptosis and induce gemcitabine resistance in pancreatic cancer cells by secreting exosome-derived ACSL4-targeting miRNAs. Drug Resist Updates: Reviews Commentaries Antimicrob Anticancer Chemother 68100960. https://doi.org/10.1016/j.drup.2023.100960
37. Pushpakom S, Iorio F, Eyers PA, Escott KJ, Hopper S, Wells A, Doig A, Guilliams T, Latimer J, McNamee C et al (2019) Drug repurposing: progress, challenges and recommendations. Nat Rev Drug Discovery 18(1):41–58. https://doi.org/10.1038/nrd.2018.168
38. Chen L, Jiang J, Dou B, Feng H, Liu J, Zhu Y, Zhang B, Zhou T, Wei G-W (2024) Machine learning study of the extended drug-target interaction network informed by pain related voltage-gated sodium channels. Pain 165(4):908–921. https://doi.org/10.1097/j.pain.0000000000003089